Journal of Power Sources 197 (2012) 88–92

Contents lists available at ScienceDirect

Journal of Power Sources

journal homepage: www.elsevier.com/locate/jpowsour

Short communication

H_2O_2 detection analysis of oxygen reduction reaction on cathode and anode catalysts for polymer electrolyte fuel cells

Akira Kishi, Sayoko Shironita, Minoru Umeda*

Department of Materials Science and Technology, Faculty of Engineering, Nagaoka University of Technology, 1603-1, Kamitomioka, Nagaoka, Niigata 940-2188, Japan

ARTICLE INFO

Article history:
Received 24 May 2011
Received in revised form 22 July 2011
Accepted 2 August 2011
Available online 9 August 2011

Keywords:
Powder electrocatalyst
H_2O_2
Oxygen reduction reaction
Porous microelectrode

ABSTRACT

The generation percentage of H_2O_2 during oxygen reduction reaction (ORR) at practical powder electrocatalysts was evaluated using a scanning electrochemical microscope (SECM). We employed a porous microelectrode that contains electrocatalysts, namely, Pt/C, Pt–Co/C, and Pt–Ru/C as the oxygen reduction electrode of the SECM, and the Pt microelectrode was used as the H_2O_2 detector. First, the H_2O_2 generation amount at Pt/Cs was measured by changing the Pt loading amount. A Pt/C with a higher Pt loading has a higher ORR activity and generates a larger amount of H_2O_2. However, the percentage of H_2O_2 generated with respect to the ORR is the same regardless of the Pt loading amount. Next, H_2O_2 generation is markedly suppressed at the Pt–Co/C and Pt–Ru/C in the potential ranges of practical fuel cell cathode and anode, respectively. This explains that the Pt–Co/C is effective when used as a cathode, and the anode Pt–Ru/C enables the reduction of the H_2O_2 generation even if O_2 crossleak occurs in the practical polymer electrolyte fuel cell.

1. Introduction

Polymer electrolyte fuel cells (PEFCs) have attracted much attention as a highly efficient power generation system for clean energy [1–4]. The oxygen reduction reaction (ORR) rate at the cathode of PEFCs is much slower than the hydrogen oxidation rate at the anode. It is therefore important to investigate the ORR at the cathode of PEFCs. During the ORR, H_2O_2 is generated as a by-product. The generated H_2O_2 degrades the polymer electrolyte membrane, the Pt-based cathode, and the carbon support of the electrocatalyst [5–7]. For this reason, it is important to study electrocatalysts that suppress the generation of H_2O_2 as a by-product.

Thus far, electrocatalysts for the cathode have been developed by adding Co, Fe, and Ni to Pt/C and also by changing the amount of Pt loading at Pt/C for practical applications [8–10]. Furthermore, H_2O_2 is generated not only at the cathode but also at the anode of PEFCs. As for the anode, H_2O_2 is generated by reacting the hydrogen fed to the anode and the oxygen crossleaked from the cathode [11]. As for anode catalysts, Pt/C and Pt–Ru/C are being investigated [12]. Although the H_2O_2 by-product is generated on these practical electrocatalysts used in PEFCs, the amount of H_2O_2 has not been analyzed in detail. Consequently, the generation rate of H_2O_2 should be quantitatively investigated at each potential of the cathode and anode of the practical PEFC.

Rotating disk electrode (RDE), rotating ring-disk electrode (RRDE), and scanning electrochemical microscope (SECM) methods have been used to investigate the generation rate of H_2O_2 that is involved in the ORR [13–16]. However, these methods require a binder resin to fix powder electrocatalysts on the rotating electrodes. The binder resin is reported to increase the generation rate of H_2O_2 [13]. Therefore, it is necessary to evaluate the generation rate of H_2O_2 at the powdered electrocatalyst without any effect of the binder resin. In our previous work, we demonstrated a suitable method of evaluating the generated H_2O_2 using the SECM equipped with a porous microelectrode (PME), in which a powder electrocatalyst is packed without a binder resin [17].

In this study, we investigated the amount of H_2O_2 generated at powder electrocatalysts for practical applications using the SECM system. The amount of H_2O_2 was evaluated at each potential of the cathode and anode. First, the Pt/C catalyst evaluation was conducted by changing the Pt loading amount. Second, the amount of H_2O_2 at the Pt–Co/C catalyst was compared with that of Pt/C as the cathode catalyst. Third, in the same manner, the Pt–Ru/C catalyst was compared with Pt/C as the anode catalyst.

2. Experimental

2.1. Powder electrocatalysts

Three Pt/Cs were used for the comparison of H_2O_2 generation in ORR. Pt/Cs (Pt: 10 wt% and 20 wt%, C: Vulcan) were purchased from ElectroChem, Inc. and Pt/C (Pt 47.2 wt%, C: Vulcan) was purchased

* Corresponding author. Tel.: +81 258 47 9323; fax: +81 258 47 9323.
E-mail address: mumeda@vos.nagaokaut.ac.jp (M. Umeda).

0378-7753/$ – see front matter © 2011 Elsevier B.V. All rights reserved.
doi:10.1016/j.jpowsour.2011.08.010

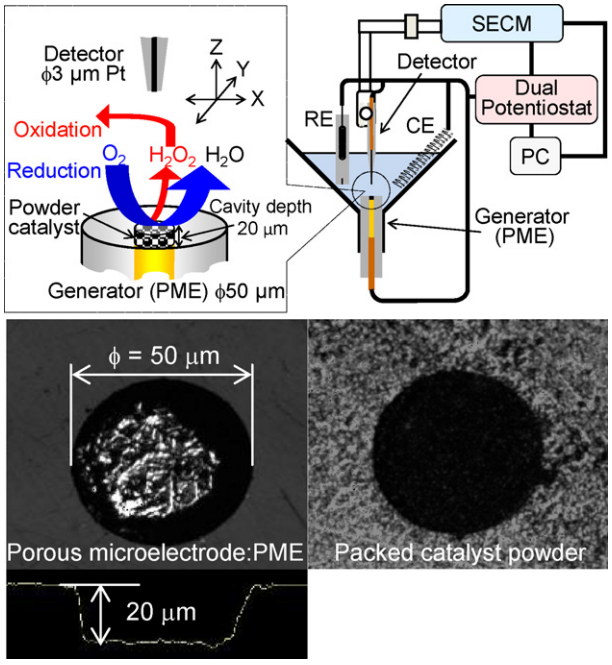

Fig. 1. Schematic of the scanning electrochemical microscope (SECM) equipped with generator and detector electrodes, and laser microscopy images before/after packed catalyst powder in porous microelectrode (PME) as the generator electrode.

from Tanaka Kikinzoku Kogyo K.K. Pt–Co/C (Pt 46.0 wt%, Co 4.6 wt%, C: Ketjen black) and Pt–Ru/C (Pt 32.6 wt%, Ru 16.9 wt%, C: Ketjen black) that were used for comparison with Pt/C (Pt 45.7 wt%, C: Ketjen black) were purchased from Tanaka Kikinzoku Kogyo K.K.

2.2. Preparation of electrodes

A porous microelectrode (PME) was prepared by the following method. A Au wire of 50 μm diameter was inserted into a glass capillary and heat-sealed by decompressing the air inside the glass. The tip of the heat-sealed capillary was then polished using lapping films. Subsequently, the tip of the Au electrode was etched in 1 mol dm^{-3} HCl aqueous solution at a current density of 0.1 A cm^{-2} for 300 s, resulting in a diameter of 50 μm and a cavity of 20 μm depth. The prepared PME was cleaned and ultrasonicated in Milli-Q water. The Pt/C electrocatalyst powder was completely filled in the microcavity of the PME so that the top of the cavity would become smooth, as shown in Fig. 1. The thus-prepared PME was used as a generator of the SECM.

The Pt microdisk electrode used as a detector of the SECM was prepared as follows. A Pt wire of 50 μm diameter was inserted into the quartz glass capillary of 1 mm diameter. Subsequently, the capillary was installed in a micropipette puller (Model P-2000, Sutter) and the Pt wire in the capillary was heat-sealed by decompressing the air inside the capillary, then both ends of the capillary were pulled while heating the Pt wire [18]. A relatively slender electrode tip was prepared. After that, the tip of the microelectrode was polished using lapping films. The obtained Pt microelectrode of 3 μm diameter (glass diameter: 30 μm) was placed on the SECM as a detector.

2.3. Electrochemical measurements

In electrochemical measurements, a Pt wire and an Ag/Ag_2SO_4 were applied as counter and reference electrodes, respectively. All electrode potentials in this report are with reference to the reversible hydrogen electrode (RHE) potential at the same temperature. Prior to the measurements, the Pt/Cs and Pt–Co/C were electrochemically cleaned in 0.5 mol dm^{-3} H_2SO_4 aqueous solution through successive potential cycles for 1 h between 0.04 and 1.4 V vs. RHE at a sweep rate of 50 mV s^{-1}. It is confirmed that there is no Pt dissolution markedly by means of electrochemical surface area (ECSA) measurement. The electrochemical cleaning of Pt–Ru/C was performed through successive potential cycles for 1 h between 0.05 and 0.7 V vs. RHE at a sweep rate of 50 mV s^{-1}, because Ru will dissolve at >0.7 V vs. RHE.

For the SECM measurements, the PME was used as a generator electrode without stirring. A 3-μm-diameter Pt microelectrode as a detector was installed on an arm of the SECM instrument (HV-404, Hokuto Denko) (Fig. 1). The electrode potentials of the generator and detector were controlled using a dual potentiostat (HA1010 mM2B, Hokuto Denko).

Prior to the SECM measurements, a background cyclic voltammogram was obtained in N_2-saturated 0.5 mol dm^{-3} H_2SO_4 using the electrochemically cleaned generator at a sweep rate of 10 mV s^{-1}. Subsequently, the electrolytic solution was saturated with O_2 gas and the ORR voltammograms were obtained with a potential sweep from the rest potential to the negative direction at a sweep rate of 1 mV s^{-1}.

The SECM measurement was carried out in O_2-saturated 0.5 mol dm^{-3} H_2SO_4. The amount of H_2O_2 by-product generated during ORR was measured in the sample generation-tip collection (SG-TC) mode by the following procedure [14–16,19]. The electrode potential of the detector was set at 1.3 V vs. RHE to detect the H_2O_2 generated during ORR at the generator. The detector was set at 10 μm above the top of the generator by detaching the detector once it attached to the glass part of generator and was moved in the *X* and *Y* directions at a rate of 10 μm s^{-1}, as shown in Fig. 1. The detector electrode was not touched with the part of electrocatalyst. The central position above the generator was determined to observe the maximum H_2O_2 current at the detector. Subsequently, the detector was moved in the *Z* direction by 50 μm (see Fig. 1). In the present study, there is no influence on the ORR current at the generator–detector distance larger than 60 μm. The ORR current at the generator decreased by 10% only when the electrodes distance was 10 μm.

3. Results and discussion

3.1. Oxygen reduction reaction at Pt/C as a function of Pt loading amount

The effect of the Pt loading amount of the Pt/C electrocatalyst on the ORR performance was investigated using the SECM with the Pt/C-packed PME as a generator electrode. Three Pt/C electrocatalysts (Pt: 10, 20, and 47.2 wt%, C: Vulcan) were used for the electrochemical measurements. Fig. 2b shows the ORR voltammograms measured at the Pt/C-packed PME in O_2-saturated 0.5 mol dm^{-3} H_2SO_4 solution. Fig. 2a shows the H_2O_2 detection currents during the ORR measured at the detector, the electrode potential of which is 1.3 V vs. RHE. From Fig. 2b, it is found that the magnitude of the diffusion-limited current increases with increasing Pt loading amount. In our previous report, the ECSA of Pt is proportional to the microcavity volume of PME [20]. The ECSA of packed Pt/C electrocatalyst is possible to become reactive sites for oxygen reduction reaction. Therefore, the increase in the diffusion-limited current is attributed to the fact that the ECSA of Pt increases with increasing Pt loading amount. These voltammograms of Pt/Cs were confirmed to have the reproducibility during the initial and after the sequence of ORR measurements.

In Fig. 2a, the H_2O_2 detection currents are shown versus the generator potential. Comparison between Fig. 2a and b reveals that the

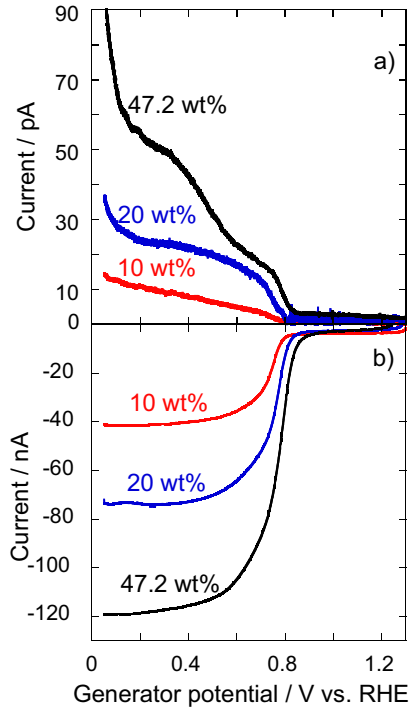

Fig. 2. Oxygen reduction *i*–*E* curves using different Pt loading amounts of Pt/C in 0.5 mol dm^{-3} H_2SO_4: (a) voltammograms of H_2O_2 detection current (detector potential: 1.3 V vs. RHE) and (b) voltammogram of ORR.

H_2O_2 detection current is <0.8 V vs. RHE, which is correlated with the ORR current. The H_2O_2 detection current also increases with increasing Pt loading amount. This suggests that the large magnitude of ORR accompanies a large amount of H_2O_2 by-product generation, which diffuses to the bulk of the electrolyte.

In Fig. 3, the H_2O_2 current is plotted versus the generator–detector distance. This measurement was performed at a generator potential of 0.6 V vs. RHE, which is nearly equal to the cathode potential of practical PEFCs. The generator–detector distance where the H_2O_2 detection current becomes zero is defined as the zero current detection point. When we compare the H_2O_2 detection current at the same generator–detector distance, the order of detection current is 47.2 > 20 > 10 wt% Pt loading amount. A electrocatalyst with a higher Pt loading generates a larger amount of H_2O_2. The zero current detection point of 10, 20, and 47.2 wt% Pt/C are found to be 160, 260, and 310 μm, respectively. Therefore, a larger amount of generated H_2O_2 increases the distance of zero current detection point.

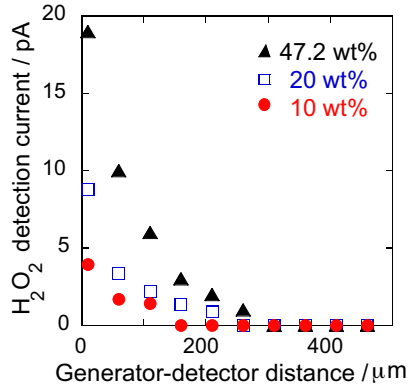

Fig. 3. H_2O_2 detection current versus the generator–detector distance using different Pt loading amounts of Pt/C at a generator potential of 0.6 V vs. RHE.

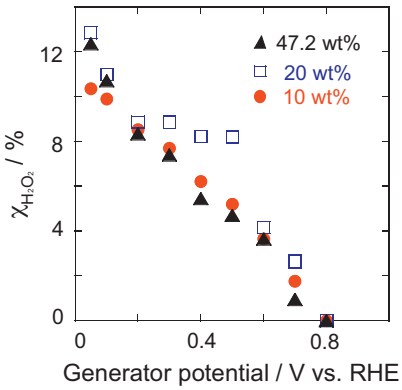

Fig. 4. Percentage of H_2O_2 versus the generator potential using three different Pt loading amounts of Pt/C.

Next, Fig. 4 shows the percentage of generated H_2O_2, $\chi_{H_2O_2}$, versus generator potential as a function of Pt loading amount. $\chi_{H_2O_2}$ was calculated at each potential using Eq. (1) [17],

$$\chi_{H_2O_2} = \frac{2I_d}{NI_g + I_d} \times 100, \quad (1)$$

where N is the collection efficiency for the SECM measurement, and the I_g and I_d are the currents observed at the generator and detector electrodes, respectively. The magnitude of N was measured using the aqueous solution including 4 mmol dm^{-3} $K_2Fe(CN)_6$ and 0.5 mol dm^{-3} K_2SO_4 and determined (N = 0.250) [17]. In Fig. 4, the plots of $\chi_{H_2O_2}$ are almost the same even when the Pt loading amount is changed. The same phenomenon is reported in the case of Pt/C using the rotating ring-disk electrode technique [21]. The result shown in Fig. 4, in which $\chi_{H_2O_2}$ is almost independent of the Pt loading amount, suggests that the ORR mechanism is unchanged even if the Pt loading amount is changed. $\chi_{H_2O_2}$ increases when the generator electrode potential shifts toward negative direction. This behavior suggests that the generated H_2O_2 adsorbed on the electrode is not stable and easily desorbs at the negative potential [22]. Therefore, the maximum $\chi_{H_2O_2}$ is observed at 0.05 V vs. RHE.

3.2. Oxygen reduction reaction at Pt–Co/C electrocatalyst

The ORR at Pt–Co/C (Pt 46.0 wt%, Co 4.6 wt%, C: Ketjen black) electrocatalyst, which is effectively used as a PEFC cathode, was compared with that at the Pt/C with the same Pt loading amount (Pt 45.7 wt%, C: Ketjen black). In this work, oxygen reduction characteristic and $\chi_{H_2O_2}$ were simultaneously evaluated with the same volume of electrocatalyst powder without any resin. Fig. 5b shows ORR voltammograms in O_2-saturated 0.5 mol dm^{-3} H_2SO_4 solution using the Pt–Co/C and Pt/C each packed in the PME. Simultaneously, the H_2O_2 detection current measured at 1.3 V vs. RHE detector potential is shown in Fig. 5a. During the measurement, the distance between the generator and detector was set as 10 μm. The magnitude of the ORR diffusion-limited current at the Pt–Co/C is as large as that observed at the Pt/C. However, the H_2O_2 detection current at the Pt–Co/C is lower than that at the Pt/C. It is reported that the effect of the added Co diminishes the desorption free energy (G_{des}) of Pt-OH, Pt-O, or Pt-O_2, such that the adsorption of oxygen containing intermediate species occurs on Pt surface sites [23]. When we consider that the practical electrode potential of the PEFC cathode is 0.6–0.9 V vs. RHE, it is shown in Fig. 5 that a small amount of H_2O_2 is generated on Pt–Co/C in the potential region. As described above, this demonstrates that the Pt–Co/C electrocatalyst is preferentially used in the PEFC cathode.

The zero current detection point of Pt–Co/C and Pt/C were measured at a generator potential of 0.6 V vs. RHE in the same way as

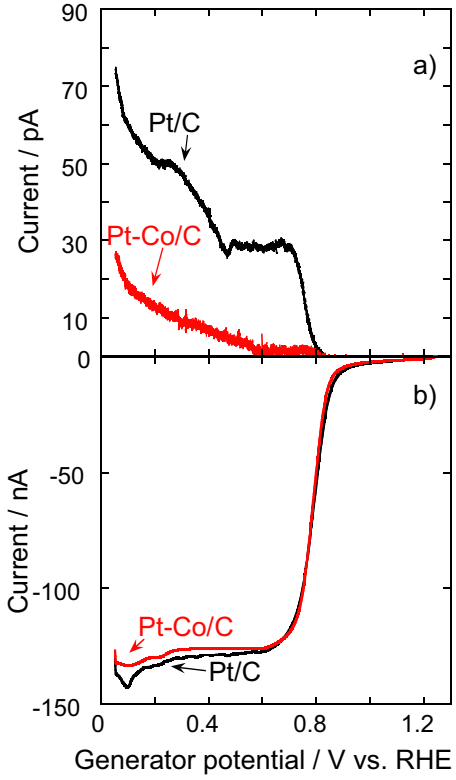

Fig. 5. Oxygen reduction *i*–*E* curves using Pt–Co/C and Pt/C in 0.5 mol dm^{-3} H_2SO_4: (a) voltammograms of H_2O_2 detection current (detector potential: 1.3 V vs. RHE) and (b) voltammogram of ORR.

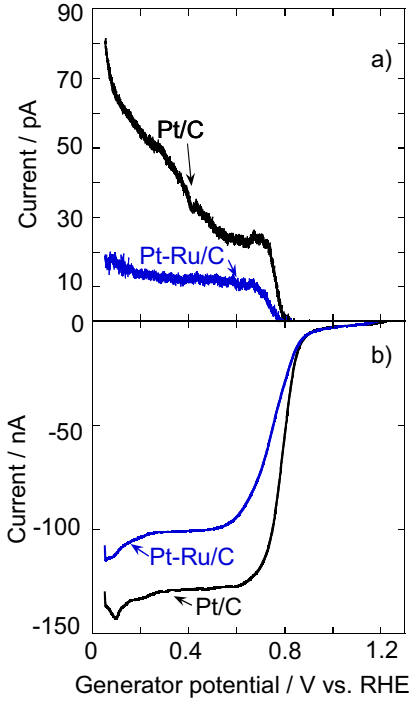

Fig. 7. Oxygen reduction *i*–*E* curves using Pt–Ru/C and Pt/C in 0.5 mol dm^{-3} H_2SO_4: (a) voltammograms of H_2O_2 detection current (detector potential: 1.3 V vs. RHE) and (b) voltammogram of ORR.

Fig. 3. The H_2O_2 detection current from Pt–Co/C is smaller than that of the Pt/C electrocatalyst. The zero current detection points of Pt–Co/C and Pt/C were 210 and 360 μm, respectively. The small H_2O_2 detection current (Fig. 5) and near zero current detection point indicate that the absolute quantity of H_2O_2 generated from Pt–Co/C is lower than that from Pt/C.

A comparison of $\chi_{H_2O_2}$, calculated using Eq. (1), for Pt–Co/C and Pt/C is shown in Fig. 6. $\chi_{H_2O_2}$ of Pt–Co/C is smaller than that of Pt/C at each generator potential. It is realized from the figure that the addition of Co to Pt suppresses the H_2O_2 generation percentage. Kadirgan et al. suggest that Co may change the local bonding geometry of Pt or the reactivity of the Pt atom by the electronic effect [24]. Therefore, the addition of Co is considered to inhibit the formation of adsorbed OH.

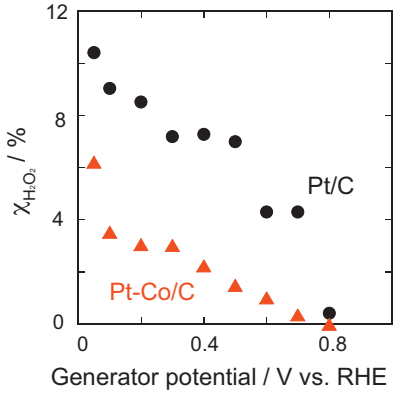

Fig. 6. Percentage of H_2O_2 versus the generator potential using Pt–Co/C and Pt/C.

3.3. Oxygen reduction reaction at Pt–Ru/C electrocatalyst

The Pt–Ru/C electrocatalyst is widely used at the PEFC anode. In this work, oxygen reduction characteristic of Pt–Ru/C was evaluated to compare with that of Pt/C at the wide potential range. Fig. 8b shows oxygen reduction voltammograms in O_2-saturated 0.5 mol dm^{-3} H_2SO_4 solution using Pt–Ru/C-packed PME and that using Pt/C for comparison. Moreover, the H_2O_2 detection currents were obtained at 1.3 V vs. RHE of detector electrode (Fig. 7a). The magnitude of the ORR diffusion-limited current at the Pt–Ru/C is smaller than that at the Pt/C. Comparison between Pt–Ru/C and Pt/C reveals that the H_2O_2 detection current of Pt–Ru/C is smaller than one third that of Pt/C in the potential region of <0.3 V vs. RHE, which corresponds to that of the PEFC anode. It is suggested that the proton adsorption might be weakened at the potential region by the addition of Ru [25].

The zero current detection point was measured by changing the distance between the generator and detector electrodes using Pt–Ru/C and Pt/C-packed PME. This measurement was performed at a generator potential of 0.05 V vs. RHE, which represents the practical anode potential of PEFC. Comparison of the H_2O_2 detection currents at the same generator–detector distance reveals that the current of the Pt–Ru/C catalyst was smaller than that of Pt/C. The zero current detection points of Pt–Ru/C and Pt/C were 260 and 410 μm, respectively. These results indicate that the H_2O_2 generation is suppressed by adding Ru in the Pt–Ru/C catalyst.

Fig. 8 shows a comparison of $\chi_{H_2O_2}$ for the Pt–Ru/C and Pt/C, revealing that the addition of Ru certainly suppresses the H_2O_2 generation. The $\chi_{H_2O_2}$ values of Pt/C and Pt–Ru/C are 10.4% and 3.6%, respectively, at 0.05 V vs. RHE. For Pt–Ru/C as the anode catalyst, the amount of H_2O_2 generation is markedly reduced. Therefore, it is considered that this Pt–Ru/C can suppress H_2O_2 generation even if O_2 crossleak occurs in the PEFC.

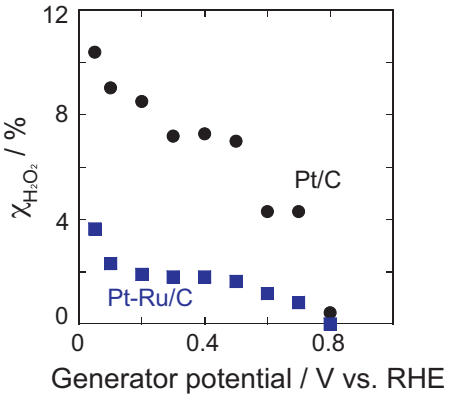

Fig. 8. Percentage of H_2O_2 versus generator potential using Pt–Ru/C and Pt/C.

4. Conclusions

$\chi_{H_2O_2}$ during ORR at practical powder electrocatalysts has been evaluated using the SECM. We employed the PME that contains the electrocatalysts of Pt/C, Pt–Co/C, and Pt–Ru/C as the oxygen reduction electrode of the SECM, and the Pt microelectrode was used as the H_2O_2 detector. First, three Pt/C electrocatalysts with the different Pt loading amounts were investigated. The Pt/C with a higher Pt loading has a higher ORR activity and generates a larger amount of H_2O_2. However, it is found that $\chi_{H_2O_2}$ with respect to the ORR is the same regardless of the Pt loading amount. Next, $\chi_{H_2O_2}$ at the Pt–Co/C and Pt–Ru/C was investigated. Results showed that $\chi_{H_2O_2}$ is markedly inhibited at the Pt–Co/C and Pt–Ru/C in the potential ranges of the practical fuel cell cathode and anode, respectively. Therefore, Pt–Co/C is suggested to be effective for H_2O_2 suppression when used as a cathode of the practical PEFC. Moreover, the anode Pt–Ru/C enables the reduction of the H_2O_2 generation even if O_2 crossleak occurs in the practical PEFC.

Acknowledgement

This work was supported by a Grant-in-Aid for Scientific Research (B, 21360358) from the Japan Society for the Promotion of Science (JSPS), Japan.

References

[1] B. Sørensen, Hydrogen and Fuel Cells: Emerging Technologies and Applications, Elsevier, Amsterdam, 2005.
[2] R.P. O'Hayre, S.W. Cha, W. Colella, F.B. Prinz, Fuel Cell Fundamentals, John Wiley & Sons, New York, 2006.
[3] K.S. Dhathathreyan, N. Rajalakshmi, in: S. Basu (Ed.), Recent Trends in Fuel Cell Science and Technology, Springer, Anamaya, 2007, p. 40.
[4] J.H. Park, P. Shakkthivel, H.J. Kim, M.K. Han, J.H. Jang, Y.R. Kim, H.S. Kim, Y.G. Shul, Int. J. Hydrogen Energy 33 (2008) 1845.
[5] F.N. Büchi, M. Inaba, T.J. Schmidt (Eds.), Polymer Electrolyte Fuel Cell Durability, Springer, New York, 2009.
[6] E. Endoh, in: W. Vielstich, H. Yokokawa, H.A. Gasteiger (Eds.), Handbook of Fuel Cells Fundamentals Technology and Applications, Vol. 5, John Wiley & Sons, Chichester, 2009, p. 359.
[7] M. Umeda, T. Maruta, M. Inoue, A. Nakazawa, J. Phys. Chem. C 112 (2008) 18098.
[8] V. Stamenković, T.J. Schmidt, P.N. Ross, N.M. Marković, J. Phys. Chem. B 106 (2002) 11970.
[9] S. Koh, J. Leisch, M.F. Toney, P. Strasser, J. Phys. Chem. C 111 (2007) 3744.
[10] H.R. Colón-Mercado, B.N. Popov, J. Power Sources 155 (2006) 253.
[11] R. Borup, J. Meyers, B. Pivovar, Y.S. Kim, R. Mukundan, N. Garland, D. Myers, M. Wilson, F. Garzon, D. Wood, P. Zelenay, K. More, K. Stroh, T. Zawodzinski, J. Boncella, J.E. McGrath, M. Inaba, K. Miyatake, M. Hori, K. Ota, Z. Ogumi, S. Miyata, A. Nishikata, Z. Shiroma, Y. Uchimoto, K. Yasuda, K. Kimijima, N. Iwashita, Chem. Rev. 107 (2007) 3904.
[12] C. Kim, Y.J. Kim, Y.A. Kim, T. Yanagisawa, K.C. Park, M. Endo, J. Appl. Phys. 96 (2004) 5903.
[13] K. Miyatake, T. Omata, D.A. Tryk, H. Uchida, M. Watanabe, J. Phys. Chem. C 113 (2009) 7772.
[14] C.M. Sánchez-Sánchez, J. Rodríguez-López, A.J. Bard, Anal. Chem. 80 (2008) 3254.
[15] Y. Shen, M. Träuble, G. Wittstock, Phys. Chem. Chem. Phys. 10 (2008) 3635.
[16] S. Kundu, T.C. Nagaiah, W. Xia, Y. Wang, S.V. Dommele, J.H. Bitter, M. Santa, G. Grundmeier, M. Bron, W. Schuhmann, M. Muhler, J. Phys. Chem. C 113 (2009) 14302.
[17] A. Kishi, M. Inoue, M. Umeda, J. Phys. Chem. C 114 (2010) 1110.
[18] T.H. Treutler, G. Wittstock, Electrochim. Acta 48 (2003) 2923.
[19] A. Kishi, T. Fukasawa, M. Umeda, J. Power Sources 195 (2010) 5996.
[20] M. Umeda, M. Kokubo, M. Mohamedi, I. Uchida, Electrochim. Acta 48 (2003) 1367.
[21] E. Higuchi, H. Uchida, M. Watanabe, J. Electroanal. Chem. 583 (2005) 69.
[22] N. Wakabayashi, M. Takeichi, H. Uchida, M. Watanabe, J. Phys. Chem. B 109 (2005) 5836.
[23] N. Ramaswamy, N. Hakim, S. Mukerjee, Electrochim. Acta 53 (2008) 3279.
[24] F. Kadirgan, A.M. Kannan, T. Atilan, S. Beyhan, S.S. Ozenler, S. Suzer, A. Yörür, Int. J. Hydrogen Energy 34 (2009) 9450.
[25] M. Inaba, M. Sugishita, J. Wada, K. Matsuzawa, H. Yamada, A. Tasaka, J. Power Sources 178 (2008) 699.